

# Pion Condensation in Baryonic Matter: from Sarma Phase to LOFF Phase

Lianyi He\*, Meng Jin† and Pengfei Zhuang‡

*Physics Department, Tsinghua University, Beijing 100084, China*

(Dated: December 2, 2024)

We investigated two pion condensed phases in the frame of two flavor Nambu–Jona-Lasinio model at finite baryon density: the homogeneous and isotropic Sarma phase and inhomogeneous and anisotropic LOFF phase. At small isospin chemical potential  $\mu_I$ , the Sarma state is free from the Sarma instability and magnetic instability due to the strong coupling and large enough effective quark mass. At large  $\mu_I$ , while the Sarma instability can be cured via fixing baryon density  $n_B$  to be nonzero, its magnetic instability implies that the LOFF state is favored than the Sarma state. In the intermediate  $\mu_I$  region, the stable ground state is the Sarma state at higher  $n_B$  and LOFF state at lower  $n_B$ .

PACS numbers: 11.30.Qc, 12.39.-x, 21.65.+f

## I. INTRODUCTION

Recently, the study on Quantum Chromodynamics (QCD) phase structure is extended to finite isospin density[1]. The physical motivation to study QCD at finite isospin density and the corresponding pion superfluidity is related to the investigation of compact stars, isospin asymmetric nuclear matter and heavy ion collisions at intermediate energies. In early studies on dense nuclear matter and compact stars, it has been suggested that charged pions are condensed at sufficiently high isospin density[2, 3, 4, 5].

While the perturbation theory of QCD can well describe the properties of new QCD phases at extremely high temperature and density, the study on the phase structure at moderate temperature and density depends on lattice QCD calculation and effective models with QCD symmetries. The lattice simulation at finite isospin chemical potential[6] shows that there is a phase transition from normal phase to pion superfluidity phase at a critical isospin chemical potential which is about the pion mass in the vacuum,  $\mu_I^c \simeq m_\pi$ . The QCD phase structure at finite isospin density is also investigated in low energy effective models, such as the Nambu–Jona-Lasinio (NJL) model applied to quarks[7, 8, 9, 10, 11, 12] which is simple but enables us to see directly how the dynamic mechanism of isospin symmetry breaking operates. In the frame of this model, it is analytically proved[10, 11] that the critical isospin chemical potential for pion superfluidity is exactly the pion mass in the vacuum,  $\mu_I^c = m_\pi$ , and this relation is independent of the model parameters and regularization scheme. In addition, near the phase transition point, the chiral and pion condensates calculated in this model are in good agreement with the lattice simulation[6]. However, up to now, most of the studies in lattice and model calculations at quark level

is done at zero baryon chemical potential, and the conditions of charge neutrality and beta equilibrium which are required in physical systems such as neutron stars can not be achieved. It is therefore necessary to study the effect of finite baryon chemical potential on the pion condensation in the frame of NJL model at quark level. Recently, this issue has been discussed in chiral limit[13].

In a pion superfluid at zero baryon chemical potential, the quark and antiquark of a condensed pair have the same isospin chemical potential and in turn the same Fermi surface (Strictly speaking, the term "Fermi surface" is only meaningful in weakly coupled fermi gas). When a nonzero baryon chemical potential is turned on, it can be regarded as a Fermi surface mismatch between the quark and antiquark. The Cooper pairing between different fermions with mismatched Fermi surfaces was discussed many years ago. In early investigation of superconductivity in an external magnetic field, Sarma found a spatially uniform state[14] where there exist gapless fermion excitations. However, compared with the fully gapped BCS state, the gapless state is energetically unfavored, which is called Sarma instability[14]. Recently, such a spatially uniform ground state prompted new interest theoretically due to the studies on fermion pairing with large mass difference[15], two-component fermionic atom gas with density difference[16, 17], isospin asymmetric nuclear matter with neutron-proton pairing[18], and neutral color superconducting quark matter[19, 20, 21, 22]. It is now generally accepted that the Sarma instability can be cured in some cases, such as the system with long-range interaction where charge neutrality is required[20, 21] and the system with proper finite range interaction between the two species of fermions with large mass difference[23]. In the Sarma state, the dispersion relation of one branch of the quasi-particles has two zero points at momenta  $p_1$  and  $p_2$  which behave as two effective Fermi surfaces, and at these two points it needs no energy for quasi-particle excitations. Since the system contains both a superfluid Fermi liquid component in the region  $p < p_1, p > p_2$  and a normal Fermi liquid component in the region  $p_1 < p < p_2$ , the Sarma state is now also called breached pairing (BP) state or interior

\*Email address: hely04@mails.tsinghua.edu.cn

†Email address: jin-m@mail.tsinghua.edu.cn

‡Email address: zhuangpf@mail.tsinghua.edu.cn

gap state.

Unfortunately, it is found that the Sarma state suffers negative superfluid density[24] or negative Meissner mass squared[25, 26] which indicates a magnetic instability, and the LOFF state[27, 28] with spatially non-uniform condensate is energetically favored than the Sarma state[29, 30, 31]. In the study of isospin asymmetric color superconducting quark matter, isospin asymmetric nuclear matter and atomic fermion gas with density difference, the LOFF phase is proposed to be the ground state and widely investigated[32, 33, 34, 35, 36]. However, it is recently argued that, the Sarma phase will be the stable ground state of asymmetric fermion superfluid in the BEC region[16, 17, 37]. In relativistic fermion superfluids, the same conclusion is obtained when the coupling is strong enough and the fermions are heavy enough[38]. While the Sarma state may not be realized in color superconductivity, since the effective quark mass is very small at large baryon density, it is probably stable in a pion condensate matter with nonzero baryon density, since the effective quark mass is large enough near the phase transition point of pion condensation, i.e., around the isospin chemical potential  $\mu_I = m_\pi$ . In this paper, we study the Sarma state and LOFF state in pion condensed matter at finite baryon density in the frame of NJL model.

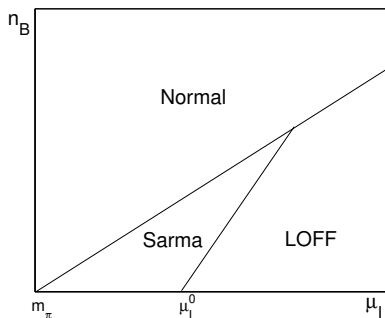


FIG. 1: The schematic phase diagram of pion condensation in the  $\mu_I - n_B$  plane.

The qualitative phase diagram of pion condensation at finite baryon density we obtained in this paper is illustrated in Fig.1 in the isospin chemical potential and baryon density plane. The pion condensation can exist when the baryon density is not very high, otherwise the system will be in normal phase without pion condensation because of the too strong mismatch. The critical baryon density for the transition from pion condensation to normal phase increases with the isospin chemical potential. The pion condensation starts at the critical value  $\mu_I^c = m_\pi$  and is separated into two phases at another critical value  $\mu_I^0$ . At small  $\mu_I$ , the Sarma phase is free from the Sarma instability and magnetic instability due to the strong coupling and large quark mass, it is therefore the stable ground state. At large  $\mu_I$ , the Sarma phase suffers

the Sarma instability and magnetic instability. While the Sarma instability can be cured via fixed nonzero baryon density, the magnetic instability implies that the LOFF phase is more favored than the Sarma phase at large  $\mu_I$ . The schematic phase diagram of pion condensation at nonzero baryon density we obtained here is similar to the phase diagram of cold polarized fermi gas proposed by Son and Stephanov[17], and the isospin chemical potential here plays the same role of the coupling in atomic fermi gas there.

The paper is organized as follows. In Section II, we review the formalism of pion condensation in the NJL model at finite isospin chemical potential and baryon chemical potential. In section III, we investigate the property of pion condensation at zero baryon chemical potential and show that there is a BEC-BCS crossover when the isospin chemical potential increases. In section IV, we evaluate the Sarma pion condensed phase and discuss the gapless quasiparticle spectrum. In section V, we study the thermodynamic stability of the Sarma phase. In section VI, we calculate the response of the Sarma phase to an external electromagnetic current and isospin current and discuss the dynamical stability of the Sarma phase. In section VII, we construct the LOFF pion condensed phase and discuss when it is more favored than the Sarma phase. We summarize in section VIII.

## II. NJL MODEL AT FINITE $\mu_I$ AND $\mu_B$

In this section, we review the formalism of NJL model at finite temperature and isospin and baryon chemical potentials[11]. Since the isospin chemical potential which triggers pion condensation is large,  $\mu_I \geq m_\pi$ , we neglect the possibility of diquark condensation which is favored at large baryon chemical potential and small isospin chemical potential. The key quantity to describe the thermodynamics of a system at finite baryon and isospin densities is the partition function defined by

$$Z(T, \mu_I, \mu_B, V) = \text{Tr} e^{-\beta(H - \mu_B B - \mu_I I_3)}, \quad (1)$$

where  $V$  is the volume of the system,  $\beta$  the inverse temperature  $\beta = 1/T$ ,  $\mu_B$  and  $\mu_I$  are the baryon and isospin chemical potentials, and  $B$  and  $I_3$  the conserved baryon number and isospin number operators. If we take only quark field  $\psi$  as elementary field of the system, the operators can be expressed as

$$B = \frac{1}{3} \int d^3\mathbf{x} \bar{\psi} \gamma_0 \psi, \quad I_3 = \frac{1}{2} \int d^3\mathbf{x} \bar{\psi} \gamma_0 \tau^3 \psi, \quad (2)$$

the factors 1/3 and 1/2 reflect the fact that 3 quarks make a baryon and quark's isospin quantum number is 1/2. In the imaginary time formalism of finite temperature field theory, the partition function can be represented as

$$Z(T, \mu_I, \mu_B, V) = \int [d\bar{\psi}][d\psi][dA] e^{-\int_0^\beta d\tau \int d^3\mathbf{x} (\mathcal{L} + \bar{\psi} \hat{\mu} \gamma_0 \psi)}, \quad (3)$$

where  $\mathcal{L}$  is the Lagrangian density describing the system, and  $\hat{\mu}$  the quark chemical potential matrix in flavor space  $\hat{\mu} = \text{diag}(\mu_u, \mu_d)$  with the  $u$  and  $d$  quark chemical potentials

$$\mu_u = \frac{\mu_B}{3} + \frac{\mu_I}{2}, \quad \mu_d = \frac{\mu_B}{3} - \frac{\mu_I}{2}. \quad (4)$$

For convenience, we also use the notation  $\mu \equiv \mu_B/3$  in the following.

The flavor  $SU(2)$  NJL Lagrangian density is defined as

$$\mathcal{L} = \bar{\psi} (i\gamma^\mu \partial_\mu - m_0) \psi + G \left[ (\bar{\psi}\psi)^2 + (\bar{\psi}i\gamma_5\tau\psi)^2 \right] \quad (5)$$

with scalar and pseudoscalar interactions corresponding to  $\sigma$  and  $\pi$  excitations. The Lagrangian density has the symmetry  $U_B(1) \otimes SU_I(2) \otimes SU_A(2)$  corresponding to baryon number symmetry, isospin symmetry and chiral symmetry, respectively. However, at nonzero isospin chemical potential, the isospin symmetry  $SU_I(2)$  breaks down to  $U_I(1)$  global symmetry with the generator  $I_3$  which is related to the condensation of charged pions. At zero baryon chemical potential, the Fermi surfaces of  $u(d)$  and anti- $d(u)$  quarks coincide and hence the condensate of  $u$  and anti- $d$  quarks is favored at sufficiently high  $\mu_I > 0$  and the condensate of  $d$  and anti- $u$  quarks is favored at sufficiently high  $\mu_I < 0$ . We introduce the chiral condensate,

$$\langle \bar{\psi}\psi \rangle = \sigma, \quad (6)$$

and the pion condensates,

$$\begin{aligned} \langle \bar{\psi}i\gamma_5\tau_+\psi \rangle &= \sqrt{2}\langle \bar{u}i\gamma_5d \rangle = \pi^+ = \frac{\pi}{\sqrt{2}}e^{i\theta}, \\ \langle \bar{\psi}i\gamma_5\tau_-\psi \rangle &= \sqrt{2}\langle \bar{d}i\gamma_5u \rangle = \pi^- = \frac{\pi}{\sqrt{2}}e^{-i\theta} \end{aligned} \quad (7)$$

with  $\tau_\pm = (\tau_1 \pm i\tau_2)/\sqrt{2}$ . A nonzero condensate  $\sigma$  means spontaneous chiral symmetry breaking, and a nonzero condensate  $\pi$  means spontaneous isospin symmetry breaking. The phase factor  $\theta$  related to the condensates  $\pi_+$  and  $\pi_-$  indicates the direction of the  $U_I(1)$  symmetry breaking. If the ground state is uniform,  $\theta$  is a constant and it does not alter the physical result. For convenience we choose  $\theta = 0$  in the following.

In mean field approximation the partition function is simplified as

$$Z(T, \mu_I, \mu_B, V) = \int [d\bar{\psi}][d\psi] e^{-\int_0^\beta d\tau \int d^3\mathbf{x} \mathcal{L}_{mf}} \quad (8)$$

with the mean field Lagrangian density

$$\mathcal{L} = \bar{\psi} [i\gamma^\mu \partial_\mu - m + \hat{\mu}\gamma_0 - i\Delta\tau_1\gamma_5] \psi - G(\sigma^2 + \pi^2), \quad (9)$$

where  $m = m_0 - 2G\sigma$  is the effective quark mass and  $\Delta = -2G\pi$  is the effective energy gap. From the mean field Lagrangian density, we can derive the inverse quark

propagator matrix in flavor space as a function of quark momentum,

$$\mathcal{S}^{-1}(p) = \begin{pmatrix} \gamma^\mu p_\mu + \mu_u \gamma_0 - m & -i\gamma_5 \Delta \\ -i\gamma_5 \Delta & \gamma^\mu p_\mu + \mu_d \gamma_0 - m \end{pmatrix}. \quad (10)$$

Using the formula listed in Appendix A, the thermodynamic potential in mean field approximation,

$$\Omega = -\frac{T}{V} \ln Z = G(\sigma^2 + \pi^2) - \frac{T}{V} \ln \det \mathcal{S}^{-1} \quad (11)$$

can be evaluated as a summation of four quasiparticle contributions,

$$\Omega = G(\sigma^2 + \pi^2) - 6 \sum_{i=1}^4 \int \frac{d^3\mathbf{p}}{(2\pi)^3} g(\omega_i(p)), \quad (12)$$

where  $\omega_i$  are the dispersions of the quasiparticles,

$$\begin{aligned} \omega_1(p) &= E_\Delta^- + \mu, & \omega_2(p) &= E_\Delta^- - \mu, \\ \omega_3(p) &= E_\Delta^+ + \mu, & \omega_4(p) &= E_\Delta^+ - \mu \end{aligned} \quad (13)$$

with the definitions

$$\begin{aligned} E_\Delta^\pm &= \sqrt{(E_p^\pm)^2 + \Delta^2}, \\ E_p^\pm &= E_p \pm \mu_I/2, \quad E_p = \sqrt{p^2 + m^2}, \end{aligned} \quad (14)$$

and the function  $g(x)$  is defined as  $g(x) = x/2 + T \ln(1 + e^{-x/T})$ . The gap equations to determine the effective quark mass  $m$  and pion condensate  $\Delta$  can be obtained by the minimum of the thermodynamic potential,

$$\frac{\partial \Omega}{\partial m} = 0, \quad \frac{\partial \Omega}{\partial \Delta} = 0, \quad \frac{\partial^2 \Omega}{\partial m^2} > 0, \quad \frac{\partial^2 \Omega}{\partial \Delta^2} > 0. \quad (15)$$

From the first order derivatives, we have

$$\begin{aligned} m - m_0 &= 12G \int \frac{d^3\mathbf{p}}{(2\pi)^3} \frac{m}{E_p} \left[ \frac{E_p^-}{E_\Delta^-} (1 - f(\omega_1) - f(\omega_2)) \right. \\ &\quad \left. + \frac{E_p^+}{E_\Delta^+} (1 - f(\omega_3) - f(\omega_4)) \right], \\ \Delta &= 12G\Delta \int \frac{d^3\mathbf{p}}{(2\pi)^3} \left[ \frac{1}{E_\Delta^-} (1 - f(\omega_1) - f(\omega_2)) \right. \\ &\quad \left. + \frac{1}{E_\Delta^+} (1 - f(\omega_3) - f(\omega_4)) \right] \end{aligned} \quad (16)$$

with the Fermi-Dirac distribution function  $f(x) = 1/(e^{x/T} + 1)$ . This group of gap equations is invariant under the transformation  $\mu_I \rightarrow -\mu_I$ , and we can only concentrate on the case  $\mu_I > 0$ . Once  $\Omega$  is known, the thermodynamic functions such as the pressure  $p$ , the entropy density  $s$ , the charge number densities  $n_B$  and  $n_I$ , the flavor number densities  $n_u$  and  $n_d$ , the energy density  $\epsilon$ , and the specific heat  $c$  can be obtained by thermodynamic relations.

To investigate the quark propagation in the pion condensed matter, we should derive the explicit form of the quark propagator at mean field level[11],

$$\mathcal{S}(p) = \begin{pmatrix} \mathcal{S}_{uu}(p) & \mathcal{S}_{ud}(p) \\ \mathcal{S}_{du}(p) & \mathcal{S}_{dd}(p) \end{pmatrix} \quad (17)$$

with the elements

$$\begin{aligned} \mathcal{S}_{uu} &= \frac{(p_0 + \mu + E_p^-) \Lambda_+ \gamma_0}{(p_0 - \omega_2)(p_0 + \omega_1)} + \frac{(p_0 + \mu - E_p^+) \Lambda_- \gamma_0}{(p_0 - \omega_4)(p_0 + \omega_3)}, \\ \mathcal{S}_{dd} &= \frac{(p_0 + \mu - E_p^-) \Lambda_- \gamma_0}{(p_0 - \omega_2)(p_0 + \omega_1)} + \frac{(p_0 + \mu + E_p^+) \Lambda_+ \gamma_0}{(p_0 - \omega_4)(p_0 + \omega_3)}, \\ \mathcal{S}_{ud} &= \frac{-i\Delta \Lambda_+ \gamma_5}{(p_0 - \omega_2)(p_0 + \omega_1)} + \frac{-i\Delta \Lambda_- \gamma_5}{(p_0 - \omega_4)(p_0 + \omega_3)}, \\ \mathcal{S}_{du} &= \frac{-i\Delta \Lambda_- \gamma_5}{(p_0 - \omega_2)(p_0 + \omega_1)} + \frac{-i\Delta \Lambda_+ \gamma_5}{(p_0 - \omega_4)(p_0 + \omega_3)}, \end{aligned} \quad (18)$$

where  $\Lambda_{\pm}$  are the energy projectors

$$\Lambda_{\pm}(\mathbf{p}) = \frac{1}{2} \left( 1 \pm \frac{\gamma_0 (\boldsymbol{\gamma} \cdot \mathbf{p} + m)}{E_p} \right). \quad (19)$$

The occupation number of each kind of quarks, namely u, d, anti-u and anti-d quarks, is useful for our discussion in the following. They can be calculated from the positive and negative energy components of the diagonal propagators  $\mathcal{S}_{uu}$  and  $\mathcal{S}_{dd}$ [11],

$$\begin{aligned} n_u^+(p) &= u_-^2 f(\omega_2) + v_-^2 f(-\omega_1), \\ n_d^-(p) &= u_-^2 f(\omega_1) + v_-^2 f(-\omega_2), \\ n_d^+(p) &= u_+^2 f(\omega_4) + v_+^2 f(-\omega_3), \\ n_u^-(p) &= u_+^2 f(\omega_3) + v_+^2 f(-\omega_4), \end{aligned} \quad (20)$$

where the symbols + and - in the notations  $n_{u,d}^{\pm}$  stand for quarks and antiquarks, respectively, and the coherent coefficients  $u_{\pm}^2$  and  $v_{\pm}^2$  are defined as

$$u_{\pm}^2 = \frac{1}{2} \left( 1 + \frac{E_p^{\pm}}{E_{\Delta}^{\pm}} \right), \quad v_{\pm}^2 = \frac{1}{2} \left( 1 - \frac{E_p^{\pm}}{E_{\Delta}^{\pm}} \right). \quad (21)$$

The number density of each kind of quarks and the total baryon number density are

$$\begin{aligned} n_{u,d}^{\pm} &= 6 \int \frac{d^3 \mathbf{p}}{(2\pi)^3} n_{u,d}^{\pm}(p), \\ n_B &= 2 \int \frac{d^3 \mathbf{p}}{(2\pi)^3} [f(\omega_2) - f(\omega_1) + f(\omega_4) - f(\omega_3)]. \end{aligned} \quad (22)$$

### III. BEC-BCS CROSSOVER AT ZERO $\mu_B$

It has been argued both in effective theory and lattice simulation that at finite but not very large isospin density and zero baryon density, the QCD matter is a pure meson matter, i.e., a Bose-Einstein condensate of charged pions. At ultra high isospin density, the matter turns to

be a Fermi liquid with quark-antiquark cooper pairing[1]. Therefore, there should be a BEC to BCS crossover when the isospin chemical potential increases. In this section we discuss the gap equations (16) at  $T = \mu_B = 0$  which has been investigated in [11] and point out that there are some signals of BEC to BCS crossover in the NJL model at finite isospin density.

Since the NJL model is non-renormalizable, we should employ a hard three momentum cutoff  $\Lambda$  to regularize the gap equations. In the following numerical calculations, we take the current quark mass  $m_0 = 5$  MeV, the coupling constant  $G = 4.93$  GeV<sup>-2</sup> and the cutoff  $\Lambda = 653$  MeV. This group of parameters ensures the pion mass  $m_{\pi} = 138$  MeV and the pion decay constant  $f_{\pi} = 93$  MeV in the vacuum. Numerical solution of the gap equations is shown in Fig.2. For  $\mu_I < m_{\pi}$  the ground state is the same as the vacuum and the isospin density keeps zero, while for  $\mu_I > m_{\pi}$  the pion condensate and isospin density become nonzero. The critical isospin chemical potential  $\mu_I^c$  is exactly the vacuum pion mass  $m_{\pi}$ , and the phase transition is of second order. Since the chiral symmetry is spontaneously broken at small  $\mu_I$  and almost restored at large  $\mu_I$ , the effective quark mass  $m$  plays an important role at small  $\mu_I$  but can be neglected at large  $\mu_I$ . In fact, the effective quark mass as a function of  $\mu_I$  at  $\mu_I > m_{\pi}$  can be well described by[11]

$$\frac{m(\mu_I)}{m(0)} \simeq \frac{\sigma(\mu_I)}{\sigma(0)} = \left( \frac{m_{\pi}}{\mu_I} \right)^2. \quad (23)$$

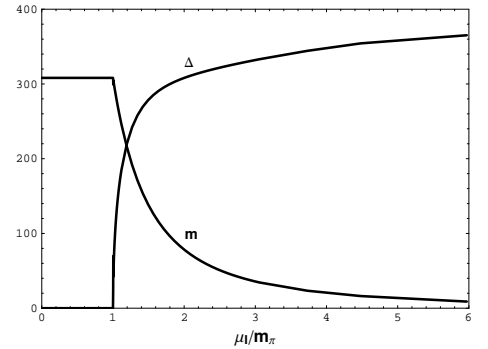


FIG. 2: The effective quark mass  $m$  and the pion condensate  $\Delta$  as functions of  $\mu_I / m_{\pi}$ .

To explain why there will be a BEC to BCS crossover, we focus firstly on the dispersion relations of the fermionic excitations,

$$\begin{aligned} \omega_{1,2}(p) &= \sqrt{\left( \sqrt{p^2 + m^2} - \mu_I/2 \right)^2 + \Delta^2}, \\ \omega_{3,4}(p) &= \sqrt{\left( \sqrt{p^2 + m^2} + \mu_I/2 \right)^2 + \Delta^2}. \end{aligned} \quad (24)$$

In the case of  $\mu_I > 0$ ,  $\omega_3 = \omega_4$  is the anti-particle excitation in the sense of isospin and irrelevant for our discussion. In Fig.3 we showed the dispersion  $\omega_1 = \omega_2$  at  $\mu_I =$

150, 450, 750 MeV. Obviously, the fermionic excitations are always gapped. At small  $\mu_I$  with  $\mu_I/2 < m(\mu_I)$ , the minimum of the dispersion is at  $p = 0$  where the energy gap is  $\sqrt{\mu_N^2 + \Delta^2}$  with  $\mu_N = \mu_I/2 - m$  which can be regarded as the corresponding non-relativistic chemical potential we will explain below. However, at large  $\mu_I$  with  $\mu_I/2 > m(\mu_I)$ , the minimum of the dispersion is shifted to  $p \simeq \mu_I/2$  where the energy gap is  $\Delta$ . This phenomenon is quite similar to the study of nucleon dispersion at finite isospin density in the nonlinear sigma model[40]. Such a phenomenon is a signal of BEC-BCS crossover.

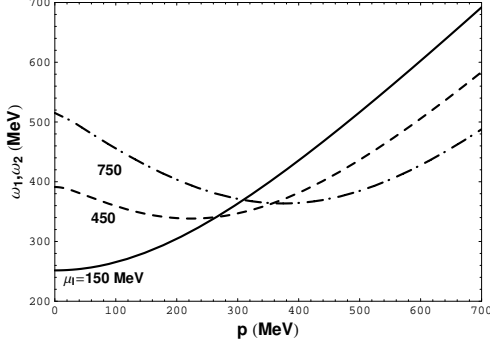


FIG. 3: The dispersion relation of the fermionic excitation  $\omega_1 = \omega_2$  at  $\mu_I = 150, 450, 750$  MeV.

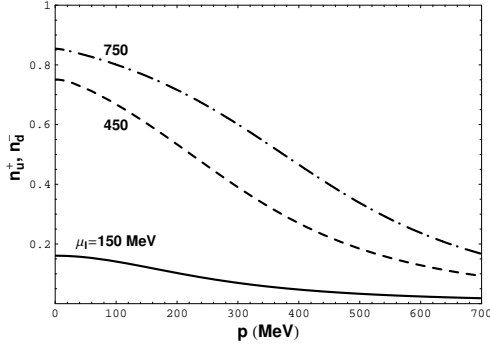


FIG. 4: The occupation number of the fermionic excitation  $n_u^+ = n_d^-$  at  $\mu_I = 150, 450, 750$  MeV.

Secondly, we discuss the occupation number of each kind of quarks ,

$$\begin{aligned} n_u^+(p) &= n_d^-(p) = v_-^2(p), \\ n_d^+(p) &= n_u^-(p) = v_+^2(p). \end{aligned} \quad (25)$$

In Fig.4 we show the occupation number  $n_u^+ = n_d^-$  at  $\mu_I = 150, 450, 750$  MeV. At small  $\mu_I$  such as  $\mu_I = 150$  MeV the occupation number is very small and smooth in the whole momentum region, while at large  $\mu_I$  the occupation number becomes large near  $p = 0$  and drops down with increasing momentum. When  $\mu_I$  becomes

very large, the occupation number is indeed of BCS type. This is the second signal of BEC-BCS crossover.

Finally, we should point out some similarity between such a BEC-BCS crossover and the non-relativistic system. For small  $\mu_I$  where  $m$  is large, the minimum of the dispersion is located at  $p = 0$ . Near this minimum with  $p \ll m$ , we can do the non-relativistic expansion

$$\sqrt{p^2 + m^2} \simeq m + \frac{p^2}{2m} + \dots, \quad (26)$$

and the corresponding non-relativistic chemical potential is

$$\mu_N = \frac{\mu_I}{2} - m. \quad (27)$$

It is well known that for a non-relativistic Fermi gas, the chemical potential will become negative in the BEC region. Therefore, we can estimate the BEC region in our model by requiring  $\mu_N < 0$ ,

$$\frac{\mu_I}{2} < m(\mu_I) = m(0) \left( \frac{m_\pi}{\mu_I} \right)^2, \quad (28)$$

which determines another critical isospin chemical potential  $\mu_I^0$  shown in the phase diagram in the introduction,

$$\mu_I^0 = [2m(0)m_\pi^2]^{1/3}. \quad (29)$$

With the above chosen parameter set, we have  $\mu_I^0 = 230$  MeV. When the effective quark mass in vacuum varies from 300 MeV to 500 MeV,  $\mu_I^0$  changes in the region 230–270 MeV. Such a non-relativistic BEC in relativistic fermion superfluid was investigated in detail in [39]. The critical value  $\mu_I^0$  we obtained here is similar to the one  $\mu_I^0 \sim (m_n m_\pi^2)^{1/3}$  obtained in nonlinear sigma model[40] where  $m_n$  is the nucleon mass. Even though the above discussion is only qualitative, it will be important for us to understand the phase structure when a nonzero baryon density is turned on.

The critical value  $\mu_I^0$  has another physical meaning. The chiral perturbation theory predicts that the chiral and pion condensates can be related to each other by a chiral rotation[1], i.e., for  $\mu_I \geq m_\pi$  there are

$$\sigma(\mu_I) = \sigma(0) \cos \alpha, \quad \pi(\mu_I) = \sigma(0) \sin \alpha \quad (30)$$

with  $\cos \alpha = m_\pi^2 / \mu_I^2$ . We found that this behavior of chiral rotation holds approximately in the region  $m_\pi < \mu_I < \mu_I^0$  and breaks down for  $\mu_I > \mu_I^0$  in the NJL model.

#### IV. SARMA PHASE AT FINITE $\mu_B$

When a baryon chemical potential is turned on, we may expect that the pion condensate will jump to zero at a critical baryon chemical potential which indicates a first order phase transition, like the behavior of chiral condensate. Such an assumption has been used in the

studies of QCD phase diagram in the NJL model[9, 12]. However, when a possible Sarma phase is taken into account, this will not be true. To see why a Sarma phase can appear, let us compare the dispersion relations of the fermionic excitations  $\omega_i$ ,  $i = 1, 2, 3, 4$  obtained here with those obtained in the study of color superconductor with charge neutrality[19]. The main differences between the two cases are 1) the averaged Fermi surface of the two paired fermions is controlled by baryon chemical potential in color superconductivity but by isospin chemical potential in pion superfluidity, and the mismatch is served by isospin chemical potential in color superconductivity but by baryon chemical potential in pion superfluidity, and 2) the effective quark mass is very small and can be neglected in color superconductivity but plays an important role in pion superfluidity when the isospin chemical potential is not too large. Taking into account these two differences, we can obtain from the conclusion for gapless color superconductivity[20] that, the Sarma phase can be realized in pion condensed matter when the gap  $\Delta$  is smaller than one third of the baryon chemical potential,  $\Delta < \mu$ .

From the possible solution of the gapless excitations,  $\omega_2(p) = 0$  and  $\omega_4(p) = 0$ , we derive the two zero points at momenta  $p_1$  and  $p_2$  satisfying  $p_1 < p_2$ ,

$$p_1 = m\sqrt{\lambda_1^2 - 1}, \quad p_2 = m\sqrt{\lambda_2^2 - 1}, \quad (31)$$

with

$$\begin{aligned} \lambda_1 &= \frac{\mu_I/2 - \sqrt{\mu^2 - \Delta^2}}{m}, \\ \lambda_2 &= \frac{\mu_I/2 + \sqrt{\mu^2 - \Delta^2}}{m}. \end{aligned} \quad (32)$$

Obviously, for  $\Delta > \mu$  or  $\Delta < \mu$  but  $|\lambda_{1,2}| < 1$ , there is no real solution of the gapless excitation, all branches of quasiparticles are gapped. In this case there are

$$\begin{aligned} n_u^+(p) &= n_d^-(p) = v_-^2, \\ n_d^+(p) &= n_u^-(p) = v_+^2 \end{aligned} \quad (33)$$

for all  $p$ , and  $n_B = 0$ . Only in the case with  $\Delta < \mu$  there is the possibility to realize the Sarma phase. According to the values of  $\lambda_{1,2}$ , there are three possible types of Sarma state.

**Type 1:**  $\lambda_1 > 0$  and  $|\lambda_{1,2}| > 1$ . In this case, only the branch  $\omega_2$  has two gapless nodes  $p_1$  and  $p_2$ , the other branches are all gapped. This case is similar to the gapless two flavor color superconductivity[20]. In this phase we have

$$\begin{aligned} n_u^+(p) &= n_d^-(p) = v_-^2, \\ n_d^+(p) &= n_u^-(p) = v_+^2 \end{aligned} \quad (34)$$

for  $p < p_1$  and  $p > p_2$  and

$$\begin{aligned} n_u^+(p) &= 1, \quad n_d^-(p) = 0, \\ n_d^+(p) &= n_u^-(p) = v_+^2 \end{aligned} \quad (35)$$

for  $p_1 < p < p_2$ . The baryon number density is

$$n_B = \frac{p_2^3 - p_1^3}{3\pi^2} = \frac{(\lambda_2^2 - 1)^{3/2} - (\lambda_1^2 - 1)^{3/2}}{3\pi^2} m^3, \quad (36)$$

the nonzero baryon number comes from the normal component in the region  $p_1 < p < p_2$ .

**Type 2:**  $|\lambda_1| < 1$  and  $|\lambda_2| > 1$ . In this case, only the branch  $\omega_2$  has one gapless node  $p_2$ , the other branches are all gapped. The system is in the paired state (34) at  $p > p_2$  and the state (35) without pairing at  $0 < p < p_2$ . The baryon number density becomes

$$n_B = \frac{p_2^3}{3\pi^2} = \frac{(\lambda_2^2 - 1)^{3/2}}{3\pi^2} m^3. \quad (37)$$

**Type 3:**  $\lambda_1 < 0$  and  $|\lambda_{1,2}| > 1$ . In this case, the branch  $\omega_2$  has a gapless node  $p_2$  and the branch  $\omega_4$  has a gapless node  $p_1$ , the other branches are all gapped. In this phase we have

$$n_u^+(p) = n_d^-(p) = v_-^2 \quad (38)$$

for  $p > p_2$  and

$$n_u^+(p) = 1, \quad n_d^-(p) = 0 \quad (39)$$

for  $0 < p < p_2$ , and

$$n_d^+(p) = n_u^-(p) = v_+^2 \quad (40)$$

for  $p > p_1$  and

$$n_d^+(p) = 1, \quad n_u^-(p) = 0 \quad (41)$$

for  $0 < p < p_1$ . The baryon number density is

$$n_B = \frac{p_1^3 + p_2^3}{3\pi^2} = \frac{(\lambda_2^2 - 1)^{3/2} + (\lambda_1^2 - 1)^{3/2}}{3\pi^2} m^3. \quad (42)$$

Before making numerical calculations, we firstly estimate where the Sarma phase is of type 2 only. From the judgement (32), it is clear that the condition to have only type 2 is  $m(\mu_I, \mu_B) > \mu_I/2$ . Since the effective quark mass at finite baryon density can not be larger than its value at zero baryon density, we have

$$\mu_I < \mu_I^0, \quad (43)$$

where  $\mu_I^0$  is the critical isospin chemical potential we obtained in last section.

Numerically solving the coupled gap equations (16) for  $m$  and  $\Delta$ , we can find all possible solutions, including the gapped and gapless (Sarma) states. At a fixed isospin chemical potential  $\mu_I$ , there is always a gapped solution  $\Delta(\mu_I, \mu_B) = \Delta(\mu_I, \mu_B = 0) \equiv \Delta_0$  provided  $\mu$  is less than the energy gap. Different from the result obtained in [13] where the gapless state can survive only in a narrow isospin chemical potential region, we found that the Sarma state can exist at any  $\mu_I > m_\pi$ . Obviously, the gap  $\Delta$  in Sarma state is smaller than the gap  $\Delta_0$  in gapped state due to the Fermi surface mismatch.

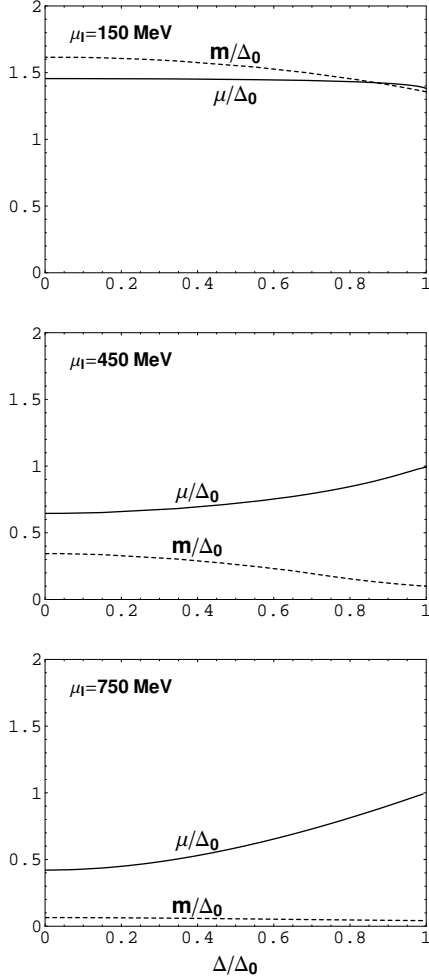


FIG. 5: The effective quark mass  $m$  and baryon chemical potential  $\mu$  as functions of the scaled pion condensate  $\Delta/\Delta_0$  at  $\mu_I = 150, 450, 750$  MeV in the gapless region.

The effective quark mass  $m$  and gap  $\Delta$  in Sarma state are shown in Fig.5 at different isospin chemical potentials. To show only the Sarma state, we have restricted the condensate in the region  $0 < \Delta/\Delta_0 < 1$ . For  $\mu_I < \mu_I^0$  such as  $\mu_I = 150$  MeV, the system is still in chiral breaking phase with large effective quark mass, and the baryon chemical potential  $\mu$  starts at a value larger than  $\Delta_0$  and then decreases slowly with increasing  $\Delta$  in the whole gapless region. The behavior that  $\mu$  decreases with  $\Delta$  is important, since it is directly related to the stability of the Sarma state, like the case in the BEC region of asymmetric fermion superfluids[16]. For  $\mu_I > \mu_I^0$  such as  $\mu_I = 450$  and  $750$  MeV, the chiral symmetry is almost restored with very small effective quark mass, and the baryon chemical potential  $\mu$  starts at a value smaller than  $\Delta_0$  and then goes up in the gapless region.

The quantities  $\lambda_1$  and  $\lambda_2$  which determine the type of the Sarma state are shown in Fig.6 as functions of the

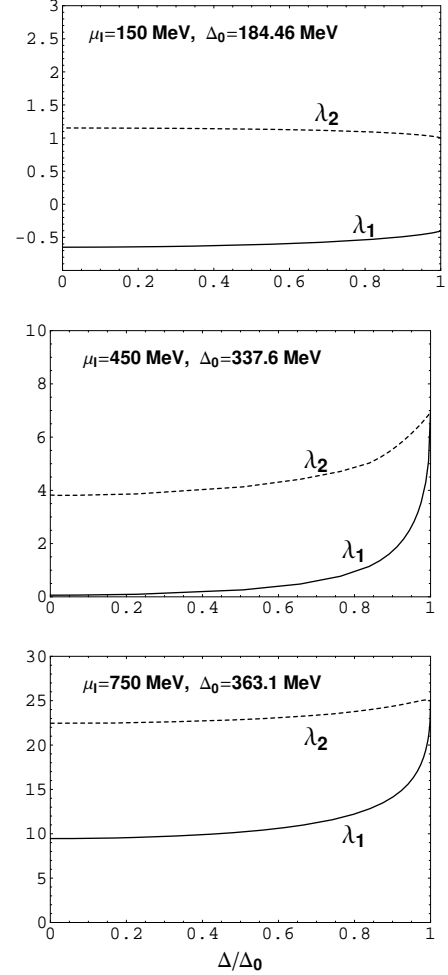


FIG. 6: The dimensionless quantities  $\lambda_1$  and  $\lambda_2$  determining the type of Sarma phase as functions of the scaled pion condensate  $\Delta/\Delta_0$  at  $\mu_I = 150, 450, 750$  MeV in the gapless region.

scaled condensate  $\Delta/\Delta_0$  at fixed isospin chemical potential. The gapless solution is of type 2 at  $\mu_I < \mu_I^0$ , as we analytically discussed above, and type 1 at large enough  $\mu_I$ . For intermediate  $\mu_I$ , there exist both type 1 at large  $\Delta$  and type 2 at small  $\Delta$ . We never found a solution of type 3. In fact, this type of Sarma phase appears only in chiral limit where the effective quark mass is always zero in pion condensation region[13].

Because of the Fermi surface mismatch in the gapless state, the baryon number density of the system is nonzero. In Fig.7 we showed the baryon density  $n_B$  as a function of  $\Delta/\Delta_0$ . It is easy to understand that  $n_B$  drops down monotonously with increasing  $\Delta$ , namely with decreasing degree of mismatch, and goes up with increasing isospin chemical potential, namely with increasing average Fermi surface. Note that the baryon density  $n_B$  and the ratio of  $n_B$  to the isospin density

$n_I$  here correspond, respectively, to the density difference and the density asymmetry  $\alpha$  in asymmetric fermion superfluids[16, 31, 41], and the ratio will decrease with increasing isospin chemical potential.

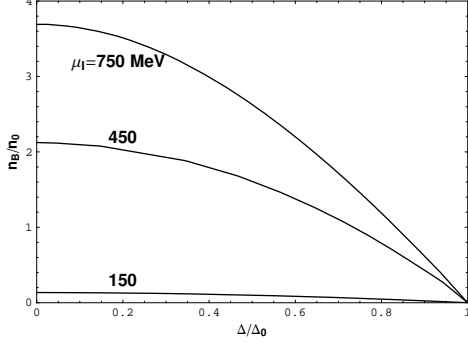


FIG. 7: The baryon number density  $n_B$  in the gapless phase, scaled by  $n_0 = 0.16fm^{-3}$ , as a function of  $\Delta/\Delta_0$  at  $\mu_I = 150, 450, 750\text{ MeV}$ .

## V. THERMODYNAMIC STABILITY

To ensure that the Sarma phase we observed in the pion condensed matter is stable, we should check both the thermodynamic and dynamical stabilities of the system[16, 42]. In this section we discuss the thermodynamic stability of the Sarma phase, i.e., the stability against a small fluctuation of the order parameter  $\Delta$ . To this end, we expand the thermodynamic potential in powers of a small fluctuation  $\delta$

$$\Omega(\Delta + \delta) - \Omega(\Delta) = \frac{\partial\Omega}{\partial\Delta}\delta + \frac{1}{2}\frac{\partial^2\Omega}{\partial\Delta^2}\delta^2 + \dots \quad (44)$$

The linear term vanishes automatically due to the gap equation  $\partial\Omega/\partial\Delta = 0$ . At zero temperature, the quantity  $\kappa_\Delta \equiv \frac{1}{6}\frac{\partial^2\Omega}{\partial\Delta^2}$  which reflects the thermodynamic stability can be directly evaluated as

$$\kappa_\Delta = \int \frac{d^3\mathbf{p}}{(2\pi)^3} \left[ \frac{\Delta^2}{(E_\Delta^-)^2} \left( \frac{\theta(\omega_2)}{E_\Delta^-} - \delta(\omega_2) \right) + (\mu_I \rightarrow -\mu_I) \right], \quad (45)$$

where  $\theta(x)$  is the step function of  $x$ . In Fig.8 we showed the scaled susceptibility  $\kappa_\Delta/\mu_I^2$  in the Sarma state as a function of the scaled pion condensate  $\Delta/\Delta_0$  at several values of  $\mu_I$ . At  $\mu_I < \mu_I^0$ ,  $\kappa_\Delta$  is always positive in the whole gapless region, which means that the Sarma state is free from the Sarma instability. In Fig.9, we plotted the thermodynamic potential at fixed baryon chemical potential as a function of the condensate, the minimum corresponds really to the Sarma state. As is well known, to have a stable Sarma state at fixed chemical potential, the system should be under some specific conditions, for instance, a proper finite range interaction between the

two species of fermions with large mass difference. Here we found a stable Sarma state at fixed chemical potential without mass difference in the frame of a four-fermion point interaction. Such a phenomenon was observed in a strong coupling model[38] and is consistent with the argument in[16, 17].

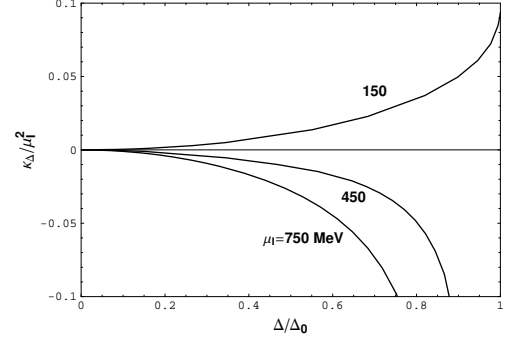


FIG. 8: The scaled susceptibility  $\kappa_\Delta/\mu_I^2$  as a function of the scaled pion condensate  $\Delta/\Delta_0$  at  $\mu_I = 150, 450, 750\text{ MeV}$ .

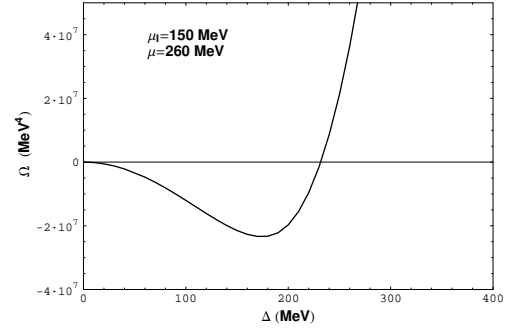


FIG. 9: The thermodynamic potential  $\Omega$  as a function of the pion condensate  $\Delta$  at fixed chemical potentials  $\mu = 260\text{ MeV}$  and  $\mu_I = 150\text{ MeV}$ .

For  $\mu_I > \mu_I^0$ , the susceptibility becomes negative and the Sarma state suffers from the thermodynamic instability. The question is, can we cure the Sarma instability at large  $\mu_I$  by considering baryon number conservation in physical systems? When the baryon number is fixed to be nonzero which is required by charge neutrality, the gapped phase is ruled out, and the possible homogeneous and isotropic ground states are only normal phase without pion condensation and Sarma phase. In this case, the Sarma state may become stable like the gapless two flavor color superconductivity[20]. Different from the system at fixed baryon chemical potential where the ground state is determined by the thermodynamic potential  $\Omega$ , the free energy  $F = \Omega + \mu_B n_B$  controls the ground state for the system at fixed baryon number density  $n_B$ . As a comparison, we plotted in Fig.10 the thermodynamic potential at a fixed baryon chemical potential  $\mu = 220\text{ MeV}$



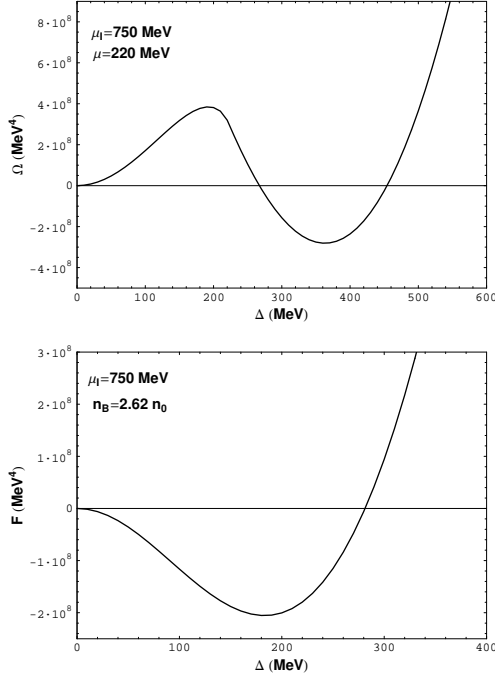


FIG. 10: The thermodynamic potential at fixed baryon chemical potential and the free energy at fixed baryon number density as functions of the pion condensate.

and the free energy  $F$  at the corresponding baryon number density  $n_B = 2.62n_0$  in the Sarma state. While the Sarma state corresponds to the maximum of the thermodynamic potential and is therefore unstable in the case at fixed chemical potential, the minimum of the free energy is located at the Sarma solution and the Sarma state is really stable in the case at fixed baryon number density.

## VI. DYNAMICAL STABILITY

We discuss now the dynamical stability of the Sarma phase, i.e., the stability against the perturbation of an external current. Since a non-zero expectation value  $\langle \bar{u}i\gamma_5 d \rangle$  breaks both electromagnetic  $U_{em}(1)$  gauge symmetry and the global  $U_I(1)$  symmetry, we will discuss the responses of the system to the external electromagnetic current  $J_{em}^\mu = e\bar{\psi}\hat{Q}\gamma^\mu\psi$  with  $\hat{Q} = \text{diag}(Q_u, Q_d)$  and to the isospin current  $J_3^\mu = \frac{1}{2}\bar{\psi}\tau_3\gamma^\mu\psi$ . The former is just the electromagnetic Meissner effect, and the later corresponds to the superfluid density which is important to judge the stability of the Sarma phase[24].

### A. Response to Electromagnetic Current

The quantity which describes the response of the system to an external electromagnetic current is the photon

self-energy or photon polarization tensor defined by

$$\Pi_{em}^{\mu\nu}(p) = -\frac{i}{2} \int \frac{d^4k}{(2\pi)^4} \text{Tr} \left[ \hat{\Gamma}_{em}^\mu \mathcal{S}(k) \hat{\Gamma}_{em}^\nu \mathcal{S}(k-p) \right] \quad (46)$$

with  $\hat{\Gamma}_{em}^\mu = e\hat{Q}\gamma^\mu$  at one loop level. In the following we discuss only the long-wave and static property of the response. The quantities that can describe this property are the Debye mass  $m_D$  and Meissner mass  $m_M$  defined as

$$m_D^2 = -\lim_{\mathbf{p} \rightarrow 0} \Pi_{em}^{00}(\omega = 0, \mathbf{p}),$$

$$m_M^2 = -\frac{1}{2} \lim_{\mathbf{p} \rightarrow 0} (g_{ij} + \hat{p}_i \hat{p}_j) \Pi_{em}^{ij}(\omega = 0, \mathbf{p}). \quad (47)$$

Since there is no possible instability associated with the Debye mass, we focus on the Meissner mass only. After some algebras, the Meissner mass can be expressed in terms of the matrix elements of the propagator  $\mathcal{S}$ ,

$$m_M^2 = \frac{3e^2}{2} \int \frac{d^3\mathbf{p}}{(2\pi)^3} \left( Q_u^2 \mathcal{T}_{uu} + Q_d^2 \mathcal{T}_{dd} + 2Q_u Q_d \mathcal{T}_{ud} \right) \quad (48)$$

with the definition

$$\mathcal{T}_{uu} = T \sum_n \text{Tr} \left( \mathcal{S}_{uu} \gamma_i \mathcal{S}_{uu} \gamma_i \right),$$

$$\mathcal{T}_{dd} = T \sum_n \text{Tr} \left( \mathcal{S}_{dd} \gamma_i \mathcal{S}_{dd} \gamma_i \right),$$

$$\mathcal{T}_{ud} = T \sum_n \text{Tr} \left( \mathcal{S}_{ud} \gamma_i \mathcal{S}_{du} \gamma_i \right), \quad (49)$$

where we should take the summation over the index  $i = 1, 2, 3$ . To avoid the UV divergence, we should subtract the vacuum contribution, which ensures that  $m_M^2$  is zero when there is no pion condensation. For  $m_M^2 > 0$ , the system exhibits diamagnetic Meissner effect, otherwise the response is paramagnetic which means a magnetic instability[25].

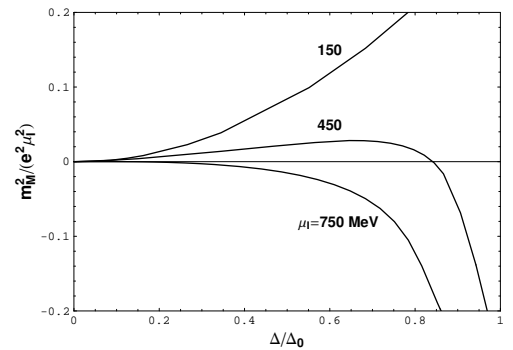


FIG. 11: The electromagnetic Meissner mass squared in the gapless state, scaled by  $e^2 \mu_I^2$ , as a function of the scaled pion condensate  $\Delta/\Delta_0$  at  $\mu_I = 150, 450, 750$  MeV.

Taking  $\mathcal{T}_{uu}$ ,  $\mathcal{T}_{dd}$  and  $\mathcal{T}_{ud}$  calculated in Appendix B, we showed in Fig.11 the Meissner mass squared  $m_M^2$  for the gapless phase at  $\mu_I = 150, 450, 750$  MeV. We found that  $m_M^2$  is positive in the whole gapless region for  $\mu_I < \mu_I^0$  which means stable Sarma state, and becomes negative in the whole region for large enough  $\mu_I$  such as  $\mu_I = 750$  MeV which indicates dynamical instability of the Sarma state. At intermediate  $\mu_I$  such as  $\mu_I = 450$  MeV, the Sarma state is stable for small gap or large baryon density and unstable for large gap or small baryon density.

### B. Response to Isospin Current

The quantity which describes the response of the system to an external isospin current is the isospin current-current correlation tensor defined by

$$\Pi_3^{\mu\nu}(p) = -\frac{i}{2} \int \frac{d^4k}{(2\pi)^4} \text{Tr} [\Gamma_3^\mu \mathcal{S}(k) \Gamma_3^\nu \mathcal{S}(k-p)] \quad (50)$$

with  $\hat{\Gamma}_3^\mu = \frac{1}{2} \tau_3 \gamma^\mu$ . We still focus on the long-wave and static property of the response by considering the quantity  $m_I^2$  defined as

$$m_I^2 = -\frac{1}{2} \lim_{\mathbf{p} \rightarrow 0} (g_{ij} + \hat{p}_i \hat{p}_j) \Pi_3^{ij}(\omega = 0, \mathbf{p}) \quad (51)$$

which is proportional to the superfluid density  $\rho_s$  of the system. After some algebras,  $m_I^2$  can be expressed in terms of the matrix elements of the propagator  $\mathcal{S}$ ,

$$m_I^2 = \frac{3}{8} \int \frac{d^3\mathbf{p}}{(2\pi)^3} (\mathcal{T}_{uu} + \mathcal{T}_{dd} - 2\mathcal{T}_{ud}). \quad (52)$$

Similarly, we should also subtract the vacuum contribution to ensure zero  $m_I^2$  in the normal phase.

We calculated numerically the mass squared  $m_I^2$  for the gapless phase at  $\mu_I = 150, 450, 750$  MeV and showed the result in Fig.12. The  $\mu_I$  dependence of the stability analysis of the Sarma state is very similar to what shown in Fig.11 for the response to the electromagnetic current.

In Figs.11 and 12, in the limit of  $\Delta/\Delta_0 \rightarrow 1$  together with  $\mu \rightarrow \Delta$ , the negative  $m_M^2$  and  $m_I^2$  behavior as  $\mu(\mu^2 - \Delta^2)^{-1/2}$  and become divergent, as observed in gapless color superconductivity[25] and breached pairing superfluidity[26]. This divergence does not appear at small  $\mu_I < \mu_I^0$ , since in the limit of  $\mu \rightarrow \Delta$ , the gapless solution does not appear due to the fact that the zero points of the excitations  $p_{1,2}$  become imaginary when  $\mu_I/2 < m$ . This behavior is quite similar to the model[38] proposed recently.

In conclusion, the Sarma pion condensed phase is always thermodynamically stable at fixed baryon number density, and dynamically stable at small isospin chemical potential  $\mu_I < \mu_I^0$  but dynamically unstable at large enough  $\mu_I$ . For intermediate  $\mu_I$  above and close to  $\mu_I^0$ , the Sarma state is stable at large baryon density and unstable at small baryon density.

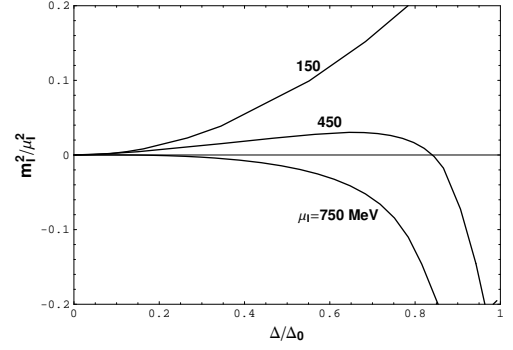


FIG. 12: The mass squared  $m_I^2$  in the gapless phase, scaled by  $\mu_I^2$ , as a function of the scaled pion condensate  $\Delta/\Delta_0$  at  $\mu_I = 150, 450, 750$  MeV.

### VII. LOFF PION CONDENSED PHASE

The order parameters  $\pi^+$  and  $\pi^-$  are complex conjugate to each other and can be set to be real only in a homogeneous and isotropic superfluid. In this section we consider the possibility that the phase factor  $\theta$  in the order parameter is non-uniform. Similar to the single plane wave LOFF state, we take the following ansatz for the pion condensate

$$\begin{aligned} \langle \bar{\psi} i \gamma_5 \tau_+ \psi \rangle &= \sqrt{2} \langle \bar{u} i \gamma_5 d \rangle = \pi^+ = \frac{\pi}{\sqrt{2}} e^{2i\mathbf{q} \cdot \mathbf{x}}, \\ \langle \bar{\psi} i \gamma_5 \tau_- \psi \rangle &= \sqrt{2} \langle \bar{d} i \gamma_5 u \rangle = \pi^- = \frac{\pi}{\sqrt{2}} e^{-2i\mathbf{q} \cdot \mathbf{x}}. \end{aligned} \quad (53)$$

We call this phase with a nonzero wave vector  $\mathbf{q}$  the LOFF pion condensed phase. Note that this phase possesses the same symmetry of the p-wave pion condensation[2, 3, 4] and is continued with the LOFF phase defined at ultra high  $\mu_I$ [1]. This phase is also similar to the chiral crystal phase[43]. After a transformation of the quark fields for each flavors,

$$\chi_u(\mathbf{x}) = u(\mathbf{x}) e^{-i\mathbf{q} \cdot \mathbf{x}}, \quad \chi_d(\mathbf{x}) = d(\mathbf{x}) e^{i\mathbf{q} \cdot \mathbf{x}}, \quad (54)$$

the Lagrangian with the new fermion fields in mean field approximation reads

$$\begin{aligned} \mathcal{L} &= \bar{\chi} [i\gamma^\mu \partial_\mu - m + \hat{\mu} \gamma_0 - \tau_3 \gamma \cdot \mathbf{q} - i\Delta \tau_1 \gamma_5] \chi, \\ &\quad - G(\sigma^2 + \pi^2) \end{aligned} \quad (55)$$

from which the inverse quark propagator matrix in the flavor space as a function of quark momentum can be derived directly,

$$\mathcal{S}^{-1}(p, \mathbf{q}) = \begin{pmatrix} \gamma^\mu p_\mu - \gamma \cdot \mathbf{q} + \mu_u \gamma_0 - m & -i\gamma_5 \Delta \\ -i\gamma_5 \Delta & \gamma^\mu p_\mu + \gamma \cdot \mathbf{q} + \mu_d \gamma_0 - m \end{pmatrix}, \quad (56)$$

and the thermodynamic potential is then expressed as

$$\Omega = G(\sigma^2 + \pi^2) - \frac{T}{V} \ln \det \mathcal{S}^{-1}. \quad (57)$$

To evaluate the thermodynamic potential, we employ the following formula which can be derived from the formula

$$[\det \mathcal{S}^{-1}]^{1/2} = \left[ (p_0 + \mu + \epsilon_-)^2 - (\epsilon_+ - \mu_I/2)^2 - \Delta^2 \right] \left[ (p_0 + \mu - \epsilon_-)^2 - (\epsilon_+ + \mu_I/2)^2 - \Delta^2 \right] + 2\Delta^2 \left[ \mathbf{p}^2 + m^2 - \mathbf{q}^2 - \sqrt{|\mathbf{p} + \mathbf{q}|^2 + m^2} \sqrt{|\mathbf{p} - \mathbf{q}|^2 + m^2} \right], \quad (58)$$

where  $\epsilon_{\pm}$  are defined as

$$\epsilon_{\pm} = \frac{1}{2} \left( \sqrt{|\mathbf{p} + \mathbf{q}|^2 + m^2} \pm \sqrt{|\mathbf{p} - \mathbf{q}|^2 + m^2} \right). \quad (59)$$

The gap equations to determine simultaneously the condensates  $m$  and  $\Delta$  and the pair momentum  $\mathbf{q}$  are derived from the minimum of the thermodynamic potential, namely the equations (15) and

$$\frac{\partial \Omega}{\partial q} = 0, \quad \frac{\partial^2 \Omega}{\partial q^2} > 0. \quad (60)$$

Numerically solving the gap equations is not a easy task due to the last term in (58). In the study of color superconductivity, people simply dropped the last term since the gap there is small but the baryon chemical potential is large[44]. Here it seems not good to employ this approximation unless  $\mu_I$  is very large. In this paper we will not directly calculate the LOFF state, but explain why the LOFF pion condensed phase is favored at large  $\mu_I$ . Following the treatment in [29, 31], we expand the thermodynamic potential in powers of the pair momentum  $\mathbf{q}$  in the vicinity of  $\mathbf{q} = 0$ ,

$$\Omega(q) - \Omega(0) = \frac{\partial \Omega}{\partial q} \Big|_{q=0} q + \frac{1}{2} \frac{\partial^2 \Omega}{\partial q^2} \Big|_{q=0} q^2 + \dots \quad (61)$$

The linear term vanishes automatically because of the gap equation (60). Separating the pair momentum dependence of the inhomogeneous quark propagator from the homogenous one,

$$\mathcal{S}^{-1}(p, \mathbf{q}) = \mathcal{S}^{-1}(p, \mathbf{q} = 0) - \tau_3 \gamma \cdot \mathbf{q}, \quad (62)$$

and taking the derivative expansion, we can easily obtain

$$\frac{\partial^2 \Omega}{\partial q^2} \Big|_{q=0} = m_I^2. \quad (63)$$

Obviously, for  $m_I^2 > 0$  at small  $\mu_I$ , the LOFF phase is less favored than the Sarma phase, and for  $m_I^2 < 0$  at large  $\mu_I$ , the LOFF phase is more favored than the Sarma phase.

From the calculation on the pion superfluidity at fixed baryon density in Section IV, we can determine the phase transition line from the pion superfluidity phase to the normal phase in the  $\mu_I - n_B$  plane at fixed temperature,

listed in Appendix A,

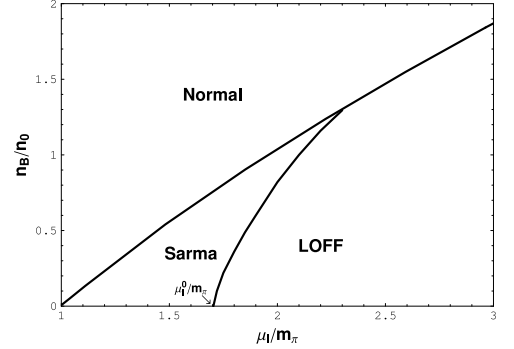


FIG. 13: The phase diagram of pion superfluidity in the  $\mu_I - n_B$  plane at zero temperature, calculated in the flavor SU(2) NJL model.

and then with the stability analysis discussed in Sections V and VI and in this section, the line which separates the inhomogeneous and anisotropic LOFF state from the homogeneous and isotropic Sarma state inside the pion superfluidity can be further fixed. The phase diagram at zero temperature is shown in Fig.13 which is very similar to the estimation Fig.1.

## VIII. SUMMARY

As a first step to achieve a physical system with pion condensate, we should consider the effect of a nonzero baryon density. In this paper we have investigated the Sarma and LOFF pion condensed matter at finite baryon number density in the frame of Nambu-Jona-Lasinio model, and checked the thermodynamic and dynamical stability of the Sarma phase.

The isospin chemical potential  $\mu_I$  controls the averaged Fermi surface of the quark-antiquark condensate, and the baryon chemical potential  $\mu_B$  offers a mismatch between the quark and antiquark. At a fixed  $\mu_I \geq \mu_I^c = m_\pi$ , the magnitude of the pion condensate decreases with increasing baryon density, and finally vanishes at a critical baryon density where the system undergoes a phase transition from the pion condensation to the normal phase. The critical baryon density increases with increasing isospin chemical potential. Inside the pion condensed

phase, the system goes from the Sarma state to the LOFF state when  $\mu_I$  increases. At low  $\mu_I \leq \mu_I^0$  where  $\mu_I^0 \sim 250$  MeV is determined by the pion mass and quark mass in the vacuum, the coupling is strong and the effective quark mass is large enough, the Sarma state is therefore thermodynamically and dynamically stable. At high enough  $\mu_I \gg \mu_I^0$ , the effective quark mass becomes very small, while the Sarma instability can be avoided via fixing the baryon number density to be nonzero, the dynamical instability of the Sarma state is still there. In this case, the LOFF state is stable. In the intermediate region with  $\mu_I$  being above and close to  $\mu_I^0$ , the stable ground state is LOFF state at lower baryon density and Sarma state at higher baryon density. The above summary of the phase structure of pion condensed matter is illustrated

in Fig.13.

Finally, we should point out that the diquark condensation in two color QCD at finite baryon density has the same behavior as the pion condensation in QCD with two or three colors at finite isospin density. This has been confirmed by both lattice simulation and low energy effective theory studies[45]. We expect that the same story will happen in two color QCD at finite baryon and isospin chemical potentials.

**Acknowledgement:** We thank Mei Huang, Judith A. McGovern, Hai-cang Ren and Igor Shovkovy for helpful discussions and comments. The work was supported in part by the grants NSFC10428510, 10435080, 10575058 and SRFDP20040003103.

## APPENDIX A: EVALUATING $\mathcal{S}^{-1}$

To evaluate the thermodynamic potential  $\Omega$  at mean field level, we should calculate the determinant of the inverse fermion propagator with off-diagonal elements

$$\mathcal{S}^{-1}(p, \mathbf{q}) = \begin{pmatrix} \mathcal{S}_1^{-1}(p, \mathbf{q}) & -i\gamma_5 \Delta \\ -i\gamma_5 \Delta & \mathcal{S}_2^{-1}(p, \mathbf{q}) \end{pmatrix}, \quad (\text{A1})$$

where

$$\mathcal{S}_\alpha^{-1}(p, \mathbf{q}) = (p_0 + \mu_\alpha)\gamma_0 - \gamma \cdot \mathbf{p}_\alpha - m_\alpha \quad (\text{A2})$$

is the inverse propagator for the quasiparticles  $\alpha = 1, 2$  with the masses  $m_1, m_2$ , the chemical potentials  $\mu_1, \mu_2$  and momenta  $\mathbf{p}_1 = \mathbf{p}_2 = \mathbf{p}$  in isotropic states and  $\mathbf{p}_1 = \mathbf{p} + \mathbf{q}$ ,  $\mathbf{p}_2 = \mathbf{p} - \mathbf{q}$  in LOFF state. Taking into account of the identity

$$\det \mathcal{S}^{-1} = \det(\gamma^5 \mathcal{S}^{-1} \gamma^5), \quad (\text{A3})$$

we have

$$\begin{aligned} \det \mathcal{S}^{-1}(p, \mathbf{q}) &= \det^{1/2} \begin{pmatrix} m_1^2 - p_1^2 - \Delta^2 & (\gamma^\mu(p_1 + p_2)_\mu - (m_1 + m_2))i\gamma_5 \Delta \\ (\gamma^\mu(p_1 + p_2)_\mu - (m_1 + m_2))i\gamma_5 \Delta & m_2^2 - p_2^2 - \Delta^2 \end{pmatrix} \\ &= [(p_1^2 - m_1^2 + \Delta^2)(p_2^2 - m_2^2 + \Delta^2) - \Delta^2((p_1 + p_2)^2 - (m_1 + m_2)^2)]^2 \end{aligned} \quad (\text{A4})$$

with  $p_\alpha = (p_0 + \mu_\alpha, \mathbf{p}_\alpha)$ . In the simplest case with  $m_1 = m_2 = m$ ,  $\mathbf{p}_1 = \mathbf{p}_2 = \mathbf{p}$  and  $\mu_1 = -\mu_2 = \mu$ , we recover the BCS type result,

$$\det \mathcal{S}^{-1}(p) = \left( p_0^2 - (\sqrt{\mathbf{p}^2 + m^2} - \mu)^2 - \Delta^2 \right)^2 \left( p_0^2 - (\sqrt{\mathbf{p}^2 + m^2} + \mu)^2 - \Delta^2 \right)^2. \quad (\text{A5})$$

## APPENDIX B: EVALUATING $\mathcal{T}_{uu}$ , $\mathcal{T}_{dd}$ AND $\mathcal{T}_{ud}$

We evaluate the quantities  $\mathcal{T}_{uu}$ ,  $\mathcal{T}_{dd}$  and  $\mathcal{T}_{ud}$  in this Appendix. Firstly we calculate the trace in the spin space. Using the relations

$$\begin{aligned} \text{Tr} [\Lambda_\pm(\mathbf{p})\gamma^0\gamma^i\Lambda_\pm(\mathbf{p})\gamma^0\gamma^i] &= 2\frac{p^2}{E_p^2}, & \text{Tr} [\Lambda_\pm(\mathbf{p})\gamma^0\gamma^i\Lambda_\mp(\mathbf{p})\gamma^0\gamma^i] &= 2\left(3 - \frac{p^2}{E_p^2}\right), \\ \text{Tr} [\Lambda_\pm(\mathbf{p})\gamma^5\gamma^i\Lambda_\pm(\mathbf{p})\gamma^5\gamma^i] &= 2\left(3 - \frac{p^2}{E_p^2}\right), & \text{Tr} [\Lambda_\pm(\mathbf{p})\gamma^5\gamma^i\Lambda_\mp(\mathbf{p})\gamma^5\gamma^i] &= 2\frac{p^2}{E_p^2}, \end{aligned} \quad (\text{B1})$$

we obtain

$$\begin{aligned}
\frac{1}{N_c} \text{Tr}(\mathcal{S}_{uu} \gamma_i \mathcal{S}_{uu} \gamma_i) &= 2 \frac{p^2}{E_p^2} \frac{(i\omega_n + \mu + E_p^-)^2}{[(i\omega_n + \mu)^2 - (E_\Delta^-)^2]^2} + 2 \frac{p^2}{E_p^2} \frac{(i\omega_n + \mu - E_p^+)^2}{[(i\omega_n + \mu)^2 - (E_\Delta^+)^2]^2} \\
&\quad + 4 \left(3 - \frac{p^2}{E_p^2}\right) \frac{i\omega_n + \mu + E_p^-}{(i\omega_n + \mu)^2 - (E_\Delta^-)^2} \frac{i\omega_n + \mu - E_p^+}{(i\omega_n + \mu)^2 - (E_\Delta^+)^2}, \\
\frac{1}{N_c} \text{Tr}(\mathcal{S}_{dd} \gamma_i \mathcal{S}_{dd} \gamma_i) &= 2 \frac{p^2}{E_p^2} \frac{(i\omega_n + \mu - E_p^-)^2}{[(i\omega_n + \mu)^2 - (E_\Delta^-)^2]^2} + 2 \frac{p^2}{E_p^2} \frac{(i\omega_n + \mu + E_p^+)^2}{[(i\omega_n + \mu)^2 - (E_\Delta^+)^2]^2} \\
&\quad + 4 \left(3 - \frac{p^2}{E_p^2}\right) \frac{i\omega_n + \mu - E_p^-}{(i\omega_n + \mu)^2 - (E_\Delta^-)^2} \frac{i\omega_n + \mu + E_p^+}{(i\omega_n + \mu)^2 - (E_\Delta^+)^2}, \\
\frac{1}{N_c} \text{Tr}(\mathcal{S}_{ud} \gamma_i \mathcal{S}_{du} \gamma_i) &= 2 \frac{p^2}{E_p^2} \frac{-\Delta^2}{[(i\omega_n + \mu)^2 - (E_\Delta^-)^2]^2} + 2 \frac{p^2}{E_p^2} \frac{-\Delta^2}{[(i\omega_n + \mu)^2 - (E_\Delta^+)^2]^2} \\
&\quad + 4 \left(3 - \frac{p^2}{E_p^2}\right) \frac{-i\Delta}{(i\omega_n + \mu)^2 - (E_\Delta^-)^2} \frac{-i\Delta}{(i\omega_n + \mu)^2 - (E_\Delta^+)^2}.
\end{aligned} \tag{B2}$$

Secondly we calculate the fermion frequency summations. From the decomposition of the summation

$$T \sum_n \frac{(i\omega_n + \mu + \epsilon)^2}{[(i\omega_n + \mu)^2 - E^2]^2} = a + (E + \epsilon)^2 b + 2\epsilon c \tag{B3}$$

for any constants  $\epsilon$  and  $E$ , and the simple frequency summations

$$\begin{aligned}
a &= T \sum_n \frac{1}{(i\omega_n + \mu)^2 - E^2} = \frac{f(E + \mu) + f(E - \mu) - 1}{2E}, \\
b &= T \sum_n \frac{1}{[(i\omega_n + \mu)^2 - E^2]^2} = \frac{1}{2E} \frac{\partial}{\partial E} \left[ \frac{f(E + \mu) + f(E - \mu) - 1}{2E} \right], \\
c &= T \sum_n \frac{1}{(i\omega_n + \mu + E)^2 (i\omega_n + \mu - E)} = \frac{f(E + \mu) + f(E - \mu) - 1}{4E^2} - \frac{1}{2E} \frac{\partial f(E + \mu)}{\partial E}
\end{aligned} \tag{B4}$$

with the definition  $f'(x) = \partial f(x)/\partial x$ , we can express some of the summations in (B2) as

$$\begin{aligned}
T \sum_n \frac{(i\omega_n + \mu + E_p^-)^2}{[(i\omega_n + \mu)^2 - (E_\Delta^-)^2]^2} &= u_-^2 v_-^2 \frac{f(\omega_1) + f(\omega_2) - 1}{E_\Delta^-} + v_-^4 f'(\omega_1) + u_-^4 f'(\omega_2), \\
T \sum_n \frac{(i\omega_n + \mu - E_p^-)^2}{[(i\omega_n + \mu)^2 - (E_\Delta^-)^2]^2} &= u_-^2 v_-^2 \frac{f(\omega_1) + f(\omega_2) - 1}{E_\Delta^-} + u_-^4 f'(\omega_1) + v_-^4 f'(\omega_2), \\
T \sum_n \frac{\Delta^2}{[(i\omega_n + \mu)^2 - (E_\Delta^-)^2]^2} &= -u_-^2 v_-^2 \frac{f(\omega_1) + f(\omega_2) - 1}{E_\Delta^-} + u_-^2 v_-^2 [f'(\omega_1) + f'(\omega_2)], \\
T \sum_n \frac{(i\omega_n + \mu + E_p^+)^2}{[(i\omega_n + \mu)^2 - (E_\Delta^+)^2]^2} &= u_+^2 v_+^2 \frac{f(\omega_3) + f(\omega_4) - 1}{E_\Delta^+} + v_+^4 f'(\omega_3) + u_+^4 f'(\omega_4), \\
T \sum_n \frac{(i\omega_n + \mu - E_p^+)^2}{[(i\omega_n + \mu)^2 - (E_\Delta^+)^2]^2} &= u_+^2 v_+^2 \frac{f(\omega_3) + f(\omega_4) - 1}{E_\Delta^+} + u_+^4 f'(\omega_3) + v_+^4 f'(\omega_4), \\
T \sum_n \frac{\Delta^2}{[(i\omega_n + \mu)^2 - (E_\Delta^+)^2]^2} &= -u_+^2 v_+^2 \frac{f(\omega_3) + f(\omega_4) - 1}{E_\Delta^+} + u_+^2 v_+^2 [f'(\omega_3) + f'(\omega_4)].
\end{aligned} \tag{B5}$$

Consider the decomposition

$$T \sum_n \frac{i\omega_n + \mu + \epsilon_1}{(i\omega_n + \mu)^2 - E_1^2} \frac{i\omega_n + \mu - \epsilon_2}{(i\omega_n + \mu)^2 - E_2^2} = d + (E_1 - \epsilon_1)(E_2 + \epsilon_2)e - (E_1 - \epsilon_1)f - (E_2 + \epsilon_2)g \tag{B6}$$

for any constants  $\epsilon_1, \epsilon_2, E_1$  and  $E_2$ , and the simple frequency summations

$$\begin{aligned}
d &= T \sum_n \frac{1}{i\omega_n + \mu - E_1} \frac{1}{i\omega_n + \mu - E_2} = \frac{1}{E_1 - E_2} [f(E_1 - \mu) - f(E_2 - \mu)], \\
e &= T \sum_n \frac{1}{(i\omega_n + \mu)^2 - E_1^2} \frac{1}{(i\omega_n + \mu)^2 - E_2^2} = \frac{1}{E_1^2 - E_2^2} \left[ \frac{f(E_1 + \mu) + f(E_1 - \mu) - 1}{2E_1} - \frac{f(E_2 + \mu) + f(E_2 - \mu) - 1}{2E_2} \right], \\
f &= T \sum_n \frac{1}{(i\omega_n + \mu)^2 - E_1^2} \frac{1}{i\omega_n + \mu - E_2} = \frac{f(E_2 - \mu)}{E_2^2 - E_1^2} + \frac{f(E_1 - \mu)}{2E_1(E_1 - E_2)} + \frac{1 - f(E_1 + \mu)}{2E_1(E_1 + E_2)}, \\
g &= T \sum_n \frac{1}{i\omega_n + \mu - E_1} \frac{1}{(i\omega_n + \mu)^2 - E_2^2} = \frac{f(E_1 - \mu)}{E_1^2 - E_2^2} + \frac{f(E_2 - \mu)}{2E_2(E_2 - E_1)} + \frac{1 - f(E_2 + \mu)}{2E_2(E_2 + E_1)},
\end{aligned} \tag{B7}$$

we can express the other summations in (B2) as

$$\begin{aligned}
& T \sum_n \frac{i\omega_n + \mu + E_p^-}{(i\omega_n + \mu)^2 - (E_\Delta^-)^2} \frac{i\omega_n + \mu - E_p^+}{(i\omega_n + \mu)^2 - (E_\Delta^+)^2} \\
&= \frac{f(\omega_2) - f(\omega_4)}{E_\Delta^- - E_\Delta^+} + \frac{(E_\Delta^- - E_p^-)(E_\Delta^+ + E_p^+)}{(E_\Delta^-)^2 - (E_\Delta^+)^2} \left[ \frac{f(\omega_1) + f(\omega_2) - 1}{2E_\Delta^-} - \frac{f(\omega_3) + f(\omega_4) - 1}{2E_\Delta^+} \right] \\
&\quad - (E_\Delta^- - E_p^-) \left[ \frac{f(\omega_4)}{(E_\Delta^+)^2 - (E_\Delta^-)^2} + \frac{f(\omega_2)}{2E_\Delta^- (E_\Delta^- - E_\Delta^+)} + \frac{1 - f(\omega_1)}{2E_\Delta^- (E_\Delta^- + E_\Delta^+)} \right] \\
&\quad - (E_\Delta^+ + E_p^+) \left[ \frac{f(\omega_2)}{(E_\Delta^-)^2 - (E_\Delta^+)^2} + \frac{f(\omega_4)}{2E_\Delta^+ (E_\Delta^+ - E_\Delta^-)} + \frac{1 - f(\omega_3)}{2E_\Delta^+ (E_\Delta^+ + E_\Delta^-)} \right], \\
& T \sum_n \frac{i\omega_n + \mu - E_p^-}{(i\omega_n + \mu)^2 - (E_\Delta^-)^2} \frac{i\omega_n + \mu + E_p^+}{(i\omega_n + \mu)^2 - (E_\Delta^+)^2} \\
&= \frac{f(\omega_2) - f(\omega_4)}{E_\Delta^- - E_\Delta^+} + \frac{(E_\Delta^- + E_p^-)(E_\Delta^+ - E_p^+)}{(E_\Delta^-)^2 - (E_\Delta^+)^2} \left[ \frac{f(\omega_1) + f(\omega_2) - 1}{2E_\Delta^-} - \frac{f(\omega_3) + f(\omega_4) - 1}{2E_\Delta^+} \right] \\
&\quad - (E_\Delta^- + E_p^-) \left[ \frac{f(\omega_4)}{(E_\Delta^+)^2 - (E_\Delta^-)^2} + \frac{f(\omega_2)}{2E_\Delta^- (E_\Delta^- - E_\Delta^+)} + \frac{1 - f(\omega_1)}{2E_\Delta^- (E_\Delta^- + E_\Delta^+)} \right] \\
&\quad - (E_\Delta^+ - E_p^+) \left[ \frac{f(\omega_2)}{(E_\Delta^-)^2 - (E_\Delta^+)^2} + \frac{f(\omega_4)}{2E_\Delta^+ (E_\Delta^+ - E_\Delta^-)} + \frac{1 - f(\omega_3)}{2E_\Delta^+ (E_\Delta^+ + E_\Delta^-)} \right], \\
& T \sum_n \frac{\Delta}{(i\omega_n + \mu)^2 - (E_\Delta^-)^2} \frac{\Delta}{(i\omega_n + \mu)^2 - (E_\Delta^+)^2} \\
&= \frac{\Delta^2}{(E_\Delta^-)^2 - (E_\Delta^+)^2} \left[ \frac{f(\omega_1) + f(\omega_2) - 1}{2E_\Delta^-} - \frac{f(\omega_3) + f(\omega_4) - 1}{2E_\Delta^+} \right].
\end{aligned} \tag{B8}$$

For a general combination

$$\mathcal{T}(\alpha, \beta) = \alpha^2 \mathcal{T}_{uu} + \beta^2 \mathcal{T}_{dd} - 2\alpha\beta \mathcal{T}_{ud}, \tag{B9}$$

we can separate it into a diamagnetic part  $\mathcal{T}_d$  and a paramagnetic part  $\mathcal{T}_p$ ,

$$\mathcal{T}(\alpha, \beta) = 2 \frac{p^2}{E_p^2} \mathcal{T}_d + 4 \left( 3 - \frac{p^2}{E_p^2} \right) \mathcal{T}_p \tag{B10}$$

with

$$\begin{aligned}
\mathcal{T}_p &= (\alpha - \beta)^2 u_-^2 v_-^2 \frac{f(\omega_1) + f(\omega_2) - 1}{E_\Delta^-} + (\alpha v_-^2 + \beta u_-^2)^2 f'(\omega_1) + (\alpha u_-^2 + \beta v_-^2)^2 f'(\omega_2) \\
&\quad + (\alpha - \beta)^2 u_+^2 v_+^2 \frac{f(\omega_3) + f(\omega_4) - 1}{E_\Delta^+} + (\alpha u_+^2 + \beta v_+^2)^2 f'(\omega_3) + (\alpha v_+^2 + \beta u_+^2)^2 f'(\omega_4), \\
\mathcal{T}_d &= \frac{1}{(E_\Delta^-)^2 - (E_\Delta^+)^2} \left[ \frac{2\alpha\beta\Delta^2 + (\alpha^2 + \beta^2)((E_\Delta^-)^2 - E_p^- E_p^+)}{2E_\Delta^-} (f(\omega_1) + f(\omega_2) - 1) - (\mu_I \rightarrow -\mu_I) \right] \\
&\quad + (\alpha^2 - \beta^2) \frac{E_\Delta^- E_p^+ - E_\Delta^+ E_p^-}{(E_\Delta^-)^2 - (E_\Delta^+)^2} \left[ \frac{f(\omega_1) + f(\omega_2) - 1}{2E_\Delta^-} - (\mu_I \rightarrow -\mu_I) \right] \\
&\quad + \frac{\alpha^2 - \beta^2}{(E_\Delta^+)^2 - (E_\Delta^-)^2} \left[ E_p^- f(\omega_4) + \frac{E_p^-}{2} \left( 1 + \frac{E_\Delta^+}{E_\Delta^-} \right) f(\omega_2) + \frac{E_p^-}{2} \left( 1 - \frac{E_\Delta^+}{E_\Delta^-} \right) (1 - f(\omega_1)) + (\mu_I \rightarrow -\mu_I) \right].
\end{aligned} \tag{B11}$$

We set  $\alpha = Q_u = 2/3$  and  $\beta = -Q_d = 1/3$  for calculating  $m_M^2$  and  $\alpha = \beta = 1$  for  $m_I^2$ . Note that only for  $\alpha = \beta$ , the formula is invariant under the exchange  $\mu_I \rightarrow -\mu_I$ , otherwise the isospin symmetry is explicitly broken.

- 
- [1] D.T.Son and M.A.Stephanov, Phys.Rev.Lett.**86**,592(2001);Phys.Atom.Nucl.**64**,834(2001). [24] S.Wu and S.Yip, Phys. Rev. **A67**, 053603(2003).
- [2] A.B.Migdal,Zh.Eksp.Teor.Fiz.61,2210(1971)(Sov.Phys.JETP **36**, 1052(1973)). [25] M.Huang and I.Shovkovy, Phys.Rev. **D70**, R051501(2004); **D70**, 094030(2004).
- [3] R.F.Sawyer, Phys.Rev.Lett.**29**,382(1972); [26] L.He, M.Jin and P.Zhuang, Phys.Rev. **B73** D.J.Scalapino,Phys.Rev.Lett.**29**,386(1972). 024511(2006).
- [4] D.K.Campbell,R.F.Dashen and J.T.Manassah, [27] A.I.Larkin and Yu.N.Ovchinnikov, Sov.Phys. JETP **20**(1965). Phys.Rev.**D12**,979(1975);**D12**,1010(1975).
- [5] D.B.Kaplan and A.E.Nelson, Phys.Lett.**B175**,57(1986). [28] P.Fulde and R.A.Ferrell,Phys. Rev **A135**,550(1964).
- [6] J.B.Kogut,D.K.Sinclair, Phys.Rev.**D66**, 034505(2002); [29] I.Giannakis and H.Ren, Phys. Lett. **B611**, 137(2005); Nucl. Phys. **B723**, 255(2005).
- [7] D.Toublan and J.B.Kogut, Phys.Lett. **B564**, 212(2003). [30] I.Giannakis, D.Hou and H.Ren, Phys.Lett. **B631** 16(2005).
- [8] M.Frank, M.Buballa and M.Oertel, Phys.Lett. **B562**, 221(2003). [31] L.He, M.Jin and P.Zhuang, Phys. Rev. **B73**, 214527(2006).
- [9] A.Barducci, R.Casalbuoni, G.Pettini, L.Ravagli, [32] M.Alford, J.Bowers and K.Rajagopal, Phys.Rev. **D63**,074016(2001). Phys.Rev. **D69**, 096004(2004); **D71**, 016011(2005).
- [10] L.He and P.Zhuang, Phys.Lett.**B615**, 93(2005); L.He, [33] R.Casalbuoni and G.Nardulli, Rev.Mod.Phys. **76**, 263(2004). M.Jin and P.Zhuang, hep-ph/0503249.
- [11] L.He, M.Jin and P.Zhuang, Phys.Rev.**D71**, 116001(2005). [34] A.Sedrakian, Phys.Rev. **C63**, 025801(2001).
- [12] H.J.Warringa, D.Boer and J.O.Andersen, [35] H.Mther and A.Sedrakian, Phys.Rev. **C67**, 015802(2003). Phys.Rev.**D72**, 014015(2005).
- [13] D.Ebert and K.G.Klimenko, J.Phys.**G32**, 599(2006); [36] A.Sedrakian, J.Mur-Petit, A.Polls and H.Mther, Phys.Rev. **A72**, 013613(2005). hep-ph/0510222.
- [14] G.Sarma, J.Phys.Chem.Solid **24**,1029(1963). [37] E.Gubankova, A.Schmitt and F.Wilczek, cond-mat/0603603.
- [15] W.V.Liu and F.Wilczek, Phys. Rev. Lett.**90**,047002(2003). [38] M.Kitazawa, D.Rischke and A.Shovkovy, hep-ph/0602065.
- [16] C.H.Pao, S.Wu and S.K.Yip, cond-mat/0506437. [39] Y.Nishida and H.Abuki, Phys.Rev. **D72**, 096004(2005).
- [17] D.T.Son and M.A.Stephanov, cond-mat/0507586. [40] Michael C. Birse, Thomas D. Cohen and Judith A. McGovern, Phys.Lett. **B516**, 27(2001).
- [18] A.Sedrakian and U.Lombardo, Phys. Rev. Lett. **84**, 602(2000). [41] H.Caldas, Phys. Rev. **A69**, 063602(2004).
- [19] M.Huang, P.Zhuang, and W.Chao, Phys. Rev. **D67**,065015(2003). [42] M.Huang, Phys.Rev. **D73**, 045007(2006).
- [20] I.Shovkovy and M.Huang, Phys. Lett. **B564**,205(2003). [43] M.Sadzikowski, Phys.Lett.**B553**, 45(2003).
- [21] M.Huang and I.Shovkovy, Nucl. Phys. **A729**,835(2003). [44] E.V.Gorbar, M.Hashimoto and V.A.Miransky, Phys.Rev.Lett. **96**, 022005 (2006).
- [22] M.Alford, C.Kouvaris and K. Rajagopal, Phys. Rev. Lett. **92**,222001(2004). [45] C.Ratti and W.Weise, Phys.Rev.**D70**, 054013(2004).
- [23] M.M.Forbes, E.Gubankova, W. Vincent Liu, F.Wilczek,